ONBOARD AUTONOMOUS GEOLOGICAL IDENTIFICATION OF ROCKS FOR PLANETARY ROVERS

Alexander Tettenborn[(1)], Alex Ellery[(1)]

[(1)]Carleton University, 1125 Colonel By Dr, Ottawa, Canada, K1S 5B6, Email: alex.tettenborn@carleton.ca, alexellery@cunet.carleton.ca

ABSTRACT

This report presents a novel approach to the problem of autonomously classifying rocks. This approach, which uses Gabor filtering in conjunction with a Gaussian naïve Bayes classifier, could be useful if deployed aboard planetary rovers, allowing them to detect and examine objects of scientific interest during the time they spend waiting for instructions from Earth based scientists. The algorithm was tested on a set of rock images by varying the number of different Gabor filters applied to each. It was found that a rectangular array of filters with 16 sinusoidal wavelengths and 26 orientations provided the best accuracy in classification at 73.3%. Increasing these parameters past this point showed a plateau in performance. This rate may indicate limitations in this method.

1. INTRODUCTION

Planetary rovers are currently limited in the amount of scientific research they can perform within their operational lifetime by constraints such as limited bandwidth, and by the long delay caused by line-of-sight communication windows between other planets and Earth [1]. If rovers could be given the tools to identify events and objects of scientific interest, their scientific productivity could be improved while decreasing earth side operational costs. A key area in detecting objects of interest is the identification and characterization of rocks through their lithological characteristics (colour, texture, grain size, stratification, etc.). Of particular interest is the identification of aqueously deposited sedimentary rocks. These are highly relevant to astrobiology and geological history as they provide insight into the history of water on Mars and are the most likely types of rock to find the organic biosignatures which would indicate past microbial life [2]. Past works have attempted to discern methods of detecting rocks on an extraterrestrial landscape using methods such as 3-dimensional surface modelling [3], intensity based image segmentation [4] and boundary and edge detection [5]. Works have also been done on autonomous classification of rocks by type using Haralick parameters [6] and expectation-maximization with Gaussian clusters [7]. This report presents a novel approach to the problem of autonomous classification which is a preliminary work in the early stage of development of an onboard autonomous geologist, suitable for deployment aboard the ExoMars rover platform (2020). This approach uses Gabor filtering at multiple scales and orientations to extract feature information from images taken by planetary rovers. These features are then used to identify and categorize geological features in the image. The use of multiple scales and orientations of Gabor filters allow this classifier to take into account visual rock characteristics such as grain size, grain distribution, bedding, rippling, vesicles, etc. This is useful as the available visual information depends highly on range and lighting conditions. Gabor filters are widely used in texture analysis and have been applied to a range of identification problems including retinal identification [8], plant leaf recognition [9] and even identifying writers of Chinese script solely by their handwriting [10]. It has been shown that image analysis using Gabor filters is similar to the way images are processed in mammalian visual systems [11]. In this report an algorithm is outlined which applies Gabor filters to extract texture information from images in order to train a Gaussian naïve Bayes classifier. This classifier is tested on a set of images of different rock types in order to determine its accuracy and effectiveness using various input parameters. The results of these tests are then presented and discussed.

2. GABOR FILTERS

The Gabor filter is an orientation sensitive linear filter used in a range of applications including edge detection, character recognition and texture analysis. It is comprised of a Gaussian kernel function modulated by a sinusoidal plane wave. When applied to an image at a particular scale and orientation, the response varies in magnitude based on the presence of spatial textures with characteristic frequencies and orientations matching the filter [12]. The formula for the Gabor filter is given in Eqs. 1-5.

$$g(x,y) = s(x,y)w(s,y) \tag{1}$$

$$s(x,y) = \exp\left(i\left(2\pi\frac{x'}{\lambda}+\varphi\right)\right) \tag{2}$$

$$w(x,y) = \exp\left(-\frac{x'^2+\gamma^2 y'^2}{2\sigma^2}\right) \tag{3}$$

$$x' = x\cos(\theta)+y\sin(\theta) \tag{4}$$

$$y' = -x\sin(\theta)=y\cos(\theta) \tag{5}$$

Where λ and φ are respectively the wavelength and phase shift of the complex sinusoidal function s, and σ and γ are respectively the standard deviation and spatial aspect ratio of the Gaussian envelope function w. θ is the normal to the parallel stripes produced by the sinusoid. When determining what features in an image will produce a response upon convolution with a Gabor filter, the most important parameters are λ and θ. The sinusoidal wavelength λ determines the scale of feature extracted by the filter, with features whose characteristic lengths are close to λ producing a larger response. The spatial orientation θ determines what angle the filter is applied at [12]. A θ value of 0 produces a filter which responds only to horizontal features, while a value of 90 responds only to vertical features. This is evident in Fig. 1 where the first filter at θ=0º and θ=45º produces a higher response to the tigers vertical stripe, than the third filter at θ=90º

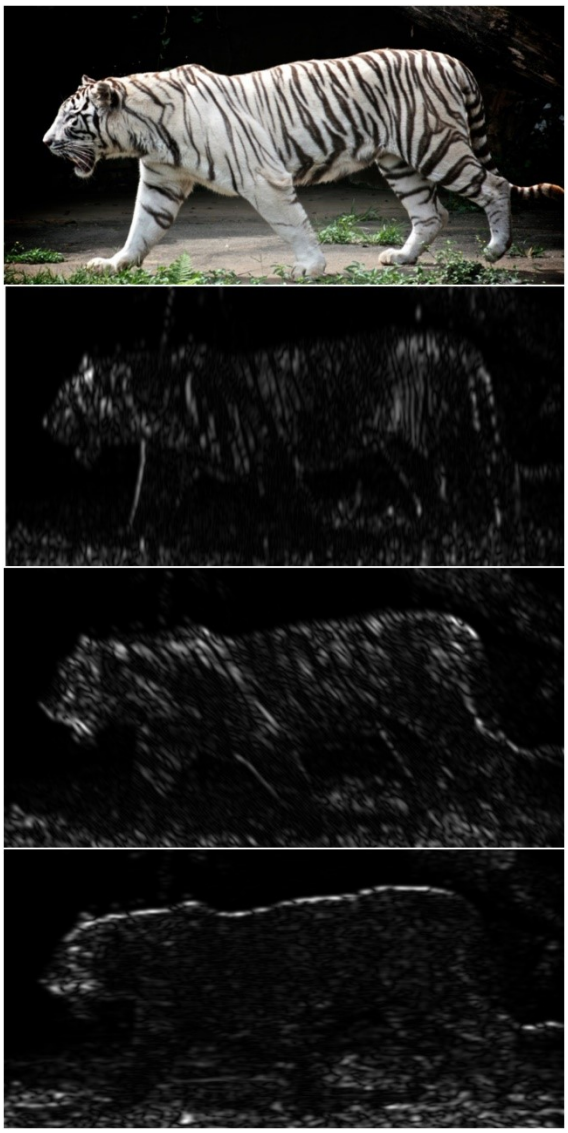

Figure 1: Image of a tiger, Gabor filtered with λ=5 pixels and θ=0, 45 and 90 degrees (top to bottom).

3. GAUSSIAN NAÏVE BAYES CLASSIFIER

A naïve Bayes classifier is a family of probabilistic classifiers which assigns a probability to each of k possible outcomes or classes, C_k given a set of n features, x_1 ,..., x_n. The probability assigned to each class is determined using Bayes' Theorem, shown in equation 6

$$p(C_k \mid x_1,...,x_n) = \frac{p(C_k)p(x_1,...,x_n \mid C_k)}{p(x_1,...,x_n)} \tag{6}$$

Making the assumption that each features is conditionally independent of all other features, Eq. 6 can equivalently be expressed as a product of the prior probability $p(C_k)$ and the likelihoods of each feature given the outcome in question. This is shown in Eq. 7.

$$p(C_k \mid x_1,...,x_n) = \frac{p(C_k)\prod_{i=1}^{n} p(x_i \mid C_k)}{p(x_1,...,x_n)} \qquad (7)$$

Because the denominator of Eq. 7 does not rely on C_k, it can be assumed to be constant. In order to find the conditional probabilities of each class, it is therefore sufficient to find the numerator of Eq. 7 for each C_k and then simply select a value for the numerator for which all probabilities sum to 1. In the case of a Gaussian naïve Bayes classifier it is assumed that that the values associated with each case follow a Gaussian distribution. If a set of data is available the parameters of these distributions can be calculated. For example, given multiple data points for attribute x in class c the mean $\mu_{c,x}$ and standard deviation $\sigma_{c,x}$ of the data implies a probability distribution given by Eq. 8.

$$p(x = v \mid c) = \frac{1}{\sqrt{2\pi\sigma_{c,x}^2}} e^{-\frac{(v-\mu_{c,x})^2}{2\sigma_{c,x}^2}} \qquad (8)$$

Given data for each class Eq. 8 can be used to determine all the feature likelihoods required by Eq. 7 in order to calculate a value of $p(C_k \mid x_1, ..., x_n)$.

4. CLASSIFIER TRAINING

In order to produce an autonomous geologist for use aboard planetary rovers, the use of Gabor filters as a texture analysis tool was tested on a set digital images of prepared rock samples, all taken from the same distance at a perpendicular angle. The set comprised 180 images, representing 21 different rock types, with between 6 and 18 images of each type. Of these images, 120 were set aside to be used as a training set for the Bayes classifier, while the remaining 60 comprised the test set.

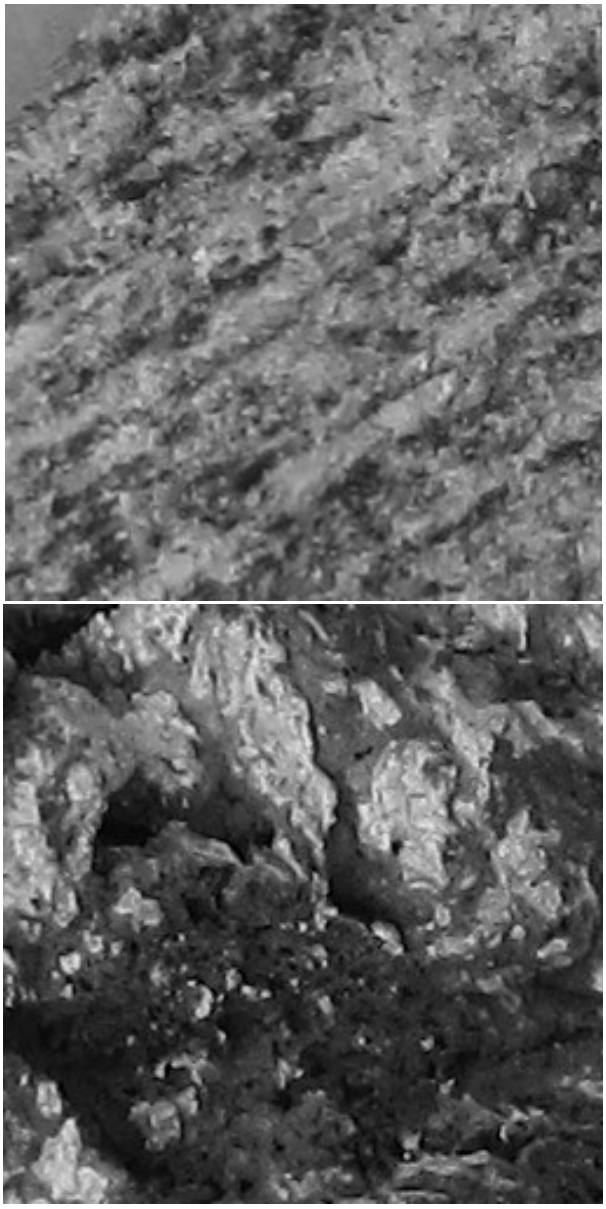

Figure 2. Grayscale images of gneiss (top) and basalt (bottom), examples of the rock images used to test the Gabor filter's texture extraction

Among the images, the orientation of striations and texture features is not constant. Two images of the same type of rock may have striations running in different direction. This mirrors the real world case as rocks on an extraterrestrial landscape will not be conveniently oriented such that texture features always have the same orientation. This means that when writing the Bayes classifier, the response to a Gabor filter at one specific

orientation and scale will not function as an effective attribute. Instead for each scale of Gabor filter applied (determined by the value of λ) the response at different orientations needs to be examined together. For the same rock sample pictured at different orientations, the peak response will occur at different values of θ, but the distribution of response should be similar, as should the peak magnitude. This is illustrated in Fig. 3 which shows the response of two images of gneiss to a Gabor filter applied at different orientations, with λ held constant. In one image the striations run approximately vertically, in the other they run at an angle approximately 60 degrees from vertical.

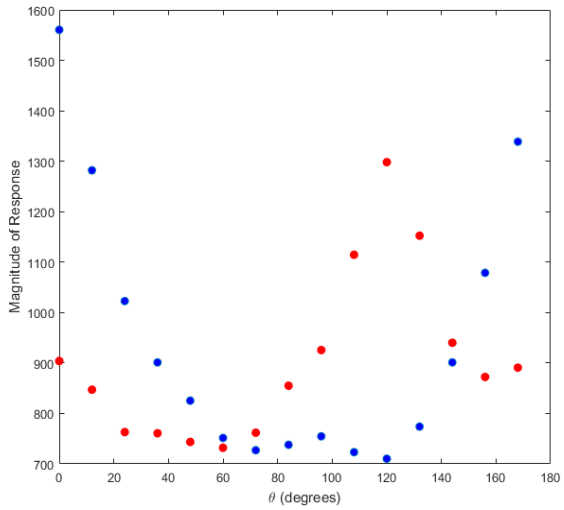

Figure 3. A comparison of the Gabor filter response at multiple orientations for two images of gneiss.

In order to train the Gaussian naïve Bayes network, an *n*-by-*m* rectangular array of Gabor filters are applied to each image with n spatial scales (different values of λ) and m orientations (different values of θ). Values of λ, given in pixels, range from 3 to 128 (half the width of the images), while values of θ range from 0 to 180 degrees. These convolutions produce, for each image, an array of complex numbers. The mean and standard deviation of the magnitude value for each image are then stored. The *i*'th spatial scale and *j*'th orientation has mean and standard deviations denoted μ_{ij} and σ_{ij}. These values are in turn used to calculate values $S_{\mu i}$ and $S_{\sigma i}$ for each spatial scale as shown in Eqs. 9-11. These represent the amount of variation in the values of μ_{ij} and σ_{ij} across the different orientations.

$$S_{\mu i} = \frac{-1}{C}\sqrt{\left(\sum_{j=1}^{m}\mu_{ij}\cos(\theta_j)\right)^2 + \left(\sum_{j=1}^{m}\mu_{ij}\sin(\theta_j)\right)^2} + \frac{1}{C} \quad (9)$$

$$S_{\sigma i} = \frac{-1}{C}\sqrt{\left(\sum_{j=1}^{m}\sigma_{ij}\cos(\theta_j)\right)^2 + \left(\sum_{j=1}^{m}\sigma_{ij}\sin(\theta_j)\right)^2} + \frac{1}{C} \quad (10)$$

$$C = 1 - \sqrt{\left(\sum_{j=1}^{m}\frac{1}{m}\cos(\theta_j)\right)^2 + \left(\sum_{j=1}^{m}\frac{1}{m}\sin(\theta_j)\right)^2} \quad (11)$$

These equations produce value which ranges from 0 in the case of all orientations having the same magnitude or standard deviation, to 1 in the case that a single magnitude or standard deviation is far greater than all the others. It can be visualized as the magnitude of the averaged position of points around a hemisphere, weighted by the corresponding μ and σ values. This method produces values dependant on the shape of the distribution, regardless of its orientation. In addition to these, the maximum value of both μ_{ij} and σ_{ij} are stored respectively as $M_{\mu i}$ and $M_{\sigma i}$ for the *i*'th value of λ. $S_{\mu i}$, $S_{\sigma i}$, $M_{\mu i}$ and $M_{\sigma i}$ then become the features in the naïve Bayes classifier, producing a final number of features equal to 4 times the number of spatial scales used.

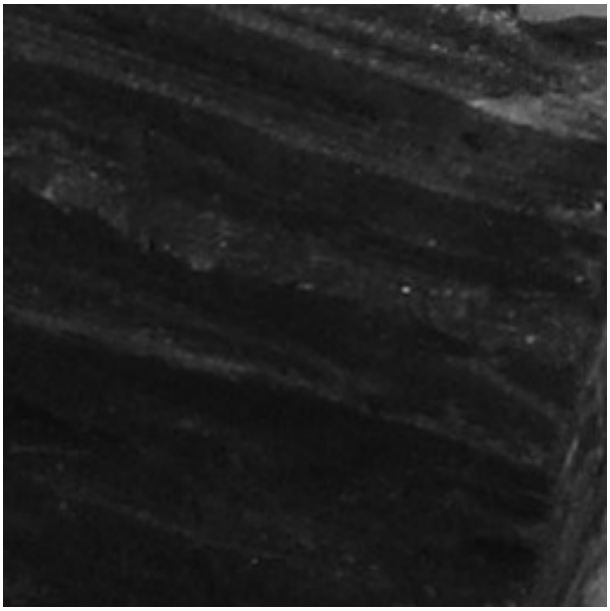

Figure 4. A grayscale image of shale, a sedimentary rock with visible striations.

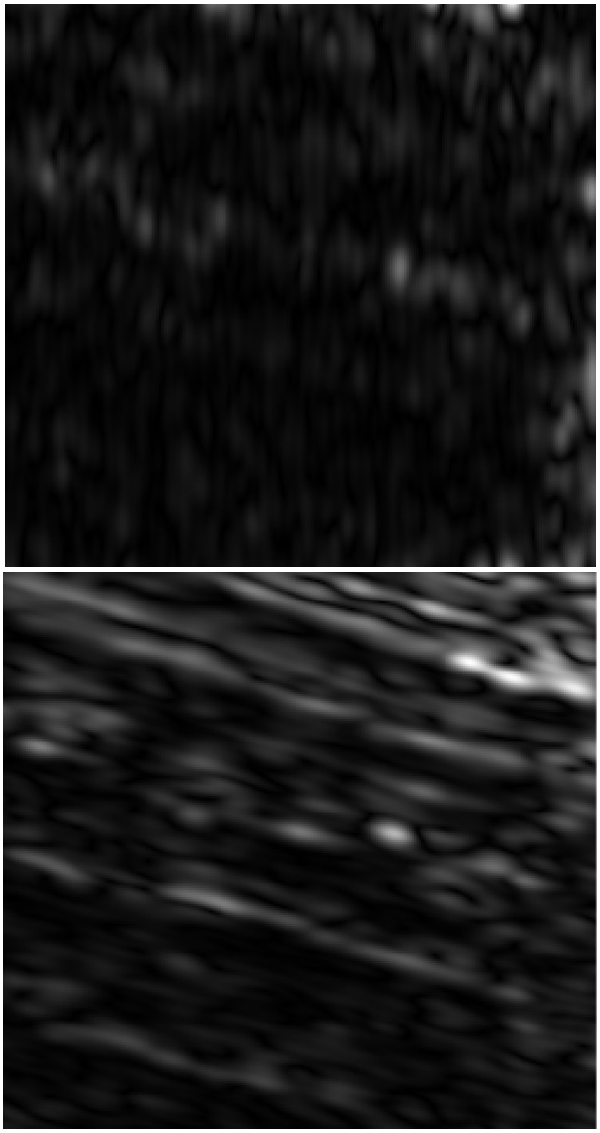

Figure 5: The Gabor response to the shale shown in Fig. 4, applied at λ=6 pixels and θ=0 and 75 degrees (top to bottom). The Gabor filter at 75 degrees shows a much greater response to the rock's striations.

In order to use a Gaussian naïve Bayes classifier, it is assumed that these features follow a Gaussian distribution. For each different rock type the mean and standard deviation of these features are calculated and used as the corresponding parameters in Eq. 8.

5. ROCK TYPE IDENTIFICATION

With a final set of means and standard deviations for the Gaussian distributions the Bayes classifier is trained and images from the test set can be identified. In order to do so the process described in section 4 is applied to the test image, producing a set of $S_{\mu i}$, $S_{\sigma i}$, $M_{\mu i}$ and $M_{\sigma i}$ for each spatial scale used. These features are then used to compute the probability of the test image belonging to each of the 21 rock types, denoted T_k, using Eq. 12.

$$p\left(T_k \mid x_1,...,x_{4n}\right) = \frac{p(T_k)\prod_{l=1}^{4n} p(x_l \mid T_k)}{p\left(x_1,...,x_{4n}\right)} \qquad (12)$$

Where n is the number of spatial scales used and the feature vector $x_1,...,x_{4n}$ is a concatenation of the sets of $S_{\mu i}$, $S_{\sigma i}$, $M_{\mu i}$ and $M_{\sigma i}$ for i from 1 to n. Each value of $p(x_l \mid T_k)$ is calculated according to Eq. 13.

$$p(x_l = x_l' \mid T_k) = \frac{1}{\sqrt{2\pi\sigma_{k,l}^2}} e^{-\frac{(x_l'-\mu_{k,l})^2}{2\sigma_{k,l}^2}} \qquad (13)$$

Where x_l' is the observed value for x_l and $\mu_{k,l}$ and $\sigma_{k,l}$ are respectively the mean and standard deviations associated with the k'th rock type and the l'th feature. With this Eq. 12 can be solved for each rock type. The denominator of Eq. 12 is selected in order to force the probabilities to sum to a value of 1. The final array of 21 probabilities is then plotted.

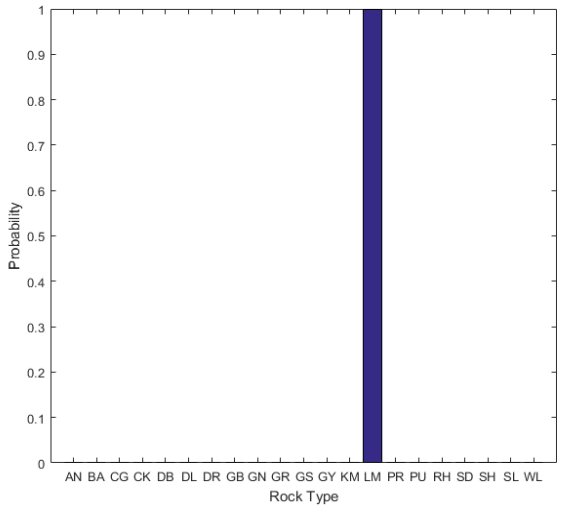

Figure 6: The resulting plot from analysis of an image of limestone. The algorithm has correctly identified the rock type.

5. RESULTS

The algorithm outlined in Chapter 3 was implemented in the MATLAB numerical computing environment. For each set of parameters used the classifier training algorithm outlined in Chapter 3 was applied to the 120 image training set in order to ready the Bayes classifier. The rock type identification outlined in chapter 5 was then applied to the remaining 60 test images after which the identification success rate was recorded. Because the Gabor filter outlined in Eqs. 1-5 do not scale uniformly when σ is changed it is preferable to express σ as a scaling directly with λ. Through experimentation it was found that the algorithm performance varied little when the ratio of σ to λ was between 1/2 and 5/2. For the results presented here a value of σ=3/2λ was used. Additionally φ and γ were found to have little effect on performance and were assigned values of 0 and 0.5 respectively. The number of λ values (n) and the number of θ values used (m) were the primary independent variables examined. The effect of orientations can also be expressed as the "orientation resolution" which refers to the angle between orientations or 360º/m.

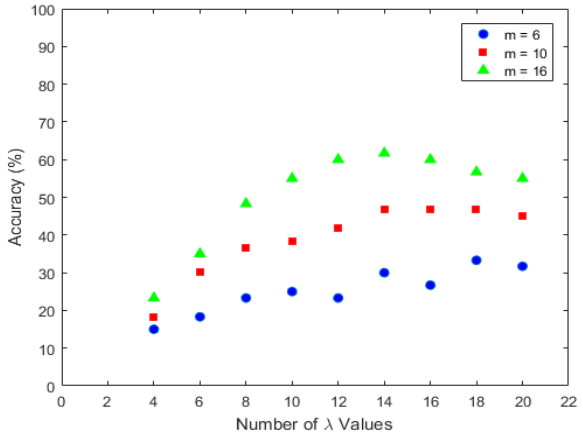

Figure 7: Results of trials varying number of λ values used in identification, with number of θ values equal to 6, 10 and 16.

Fig. 7 shows how the accuracy of the identification algorithm varies as n is varied. It can be seen regardless of the number of θ values used accuracy seems to reach a plateau around n=14. For m=16 the accuracy actually seems to decline past n=14. This result is unexpected. If this is a real phenomenon, rather than a result of some error in the code, the mechanism behind it has not yet been determined. One conjecture is that an anomalous effect is occurring when Gabor filters with large values of λ are applied. This could affect the accuracy of the detection algorithm. Higher values of n could be introducing more filters with λ high enough to produce this effect, thus slightly lowering the overall detection rate. This possibility will be further pursued in future work. Fig. 8 shows how the accuracy of the identification algorithm varies as m is varied. Again, we can see that the accuracy seems to hit a plateau, regardless of the value of n used, somewhere between m=20 and m=24. This corresponds to angular resolutions of 9º to 7.5º. A maximum detection rate of 73.3% occurred with n=16 and m=26. These results may indicate limitations to the method of rock identification outlined here. It may be that Gabor filtering do not adequately extract and isolate the common features found in these rocks types. The visual features of some rock types can vary significantly among individual samples. More sophisticated methods of identification may be necessary. Additionally, it is possible that the assumption that the features extracted by the Gabor filters follow a Gaussian distribution is false.

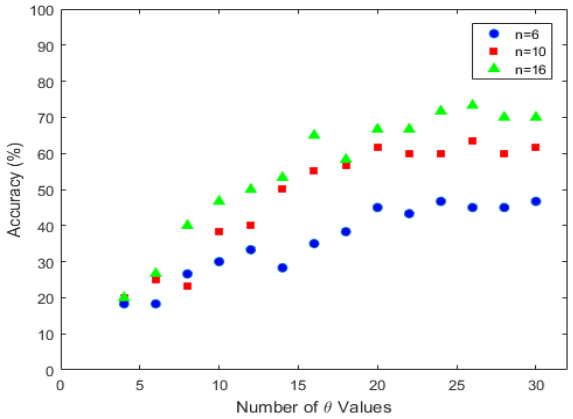

Figure 8: Results of trials varying number of θ values used in identification, with number of λ values equal to 6, 10 and 16.

6. CONCLUSION AND FUTURE WORK

In this work a method of rock identification was presented for possible use aboard planetary rovers. This method is based on Gabor filtering and Gaussian naïve Bayes classification. A set of 120 sample images of 21 different types of rock were used to examine its accuracy. It was found that the parameters most relevant to the rate of accurate detection were the number of values of λ (the wavelength of the Gabor function's sinusoidal component) and the number of values of θ (the angle at which the Gabor filter is applied) used by the algorithm. It was observed that past 14 values of λ and 24 values of θ, the detection rate reaches a plateau and stops increasing. In some cases an unexplained decrease in accuracy was seen upon increasing the number of λ values used. The maximum accuracy of 73.3% was found using 16 values of λ and 26 values of θ. This shows that the algorithm is capable of producing accurate detection in a majority of cases, but it also indicates that the methods described here may have limitations. In future work we will attempt to improve this detection rate. We plan to examine the use of wavelet transforms in place of Gabor filtering. Past experiments have shown that this method can produce high accuracy in texture classification [13]. We also plan to investigate the use of neural networks as a more robust classifier than the simpler naïve Bayes. Once a robust and reliable classification algorithm is found it will then be applied to the problem of in-the-field rock detection and characterization, where we do not have the convenience of imaging prepared rock samples from a constant angle and distance. In the end we will produce a software architecture suitable to be placed on a planetary rover to allow it to autonomously select targets of scientific interest and investigate them without the need for human intervention.

REFERENCES

1. Horne, W.D., Hastrup, R., and Cesarone, R. (1997). Telecommunications for Mars Rovers and Robotics Missions. *Space Technology* **17,** 205-213.

2. Westall, F., Foucher, F., Bost, N., Bertrand, M., Loizeau, D., Vago, J., Kminek, G., Gaboyer, F., Campbell, K., Breheret, J., Gautret, P., Cockell, C. (2015) Biosignatures on Mars: What, Where, and How? Implications for the Search for Martian Life. *Astrobiology* **15(11)**, 998-1029.

3. Li, R., Di, K., Howard, A., Matthies, L., Wang, J. (2007) Rock Modeling and Matching for Autonomous Long-Range Mars Rover Localization. *Journal of Field Robotics* **24(3)** 187-203

4. Castano, A., Anderson, C., Castano, R., Estlin, T., Judd, M. (2004) Intensity-Based Rock Detection for Acquiring Onboard Rover Science. *35th Lunar and Planetary Science Conference Proceedings*

5. Gui, C., Li, Z. (2013) An Autonomous Rock Identification Method for Planetary Exploration. *Emerging Technologies for Information Systems, Computing and Management* **236**

6. Sharif, H., Ralchenko, M., Samson, C., Ellery, A. (2015) Autonomous Rock Classification Using Bayesian Image Analysis for Rover-Based Planetary Exploration. *Computers and Geoscience* **83**, 153-167

7. Niekum, S. (2005) Reliable Rock Detection and Classification for Autonomous Science. *Masters Thesis*, Carnegie Mellon University, Pittsburgh, USA.

8. Meng, X., Yilong, Y., Yang, G., Xiaoming, X. (2013) Retinal Identification Based on an Improved Circular Gabor Filter and Scale Invariant Feature Transform. *Sensors (Basel, Switzerland)* **13(7)** 9248-9266.

9. Chaki, J., Parekh, R. (2012) Plant Leaf Recognition using Gabor Filter. *International Journal of Computer Applications* **56(10)** 26-29.

10. Wei, L., Wang, F., Dexian, Z., Zhixiao, Y., Zhiyan, Z., Fei, S. (2008) The Application of Gabor Filter in Chinese Writer Identification. *Proceedings of 2008 IEEE International Symposium on IT in Medicine and Education* pp360-362

11. Marcelja, S. (1980) Mathematical Description of the Responses of Simple Cortical Cells. *Journal of the Optical Society of America* **70**, 1297-1300

12. Moreno, P., Bernardino, A., Santos-Victor, J. (2005) Gabor Parameter Selection for Local Feature Detection. *Proceedings of 2nd Iberian Conference on Pattern Recognition and Image Analysis* pp11-19

13. Wang, Z., Yong, J. (2008) Texture Analysis and Classification With Linear Regression Model Based on Wavelet Transform. *IEEE Transactions on Image Processing* **17(8)** 1421-1430